Studia Geotechnica et Mechanica, 2024; 46(3): 164–175

Original Study **Open Access**

Paweł Siemaszko*

Pile–Soil Interaction during Static Load Test

https://doi.org/10.2478/sgem-2024-0010
received August 31, 2023; accepted May 15, 2024.

Abstract: This study highlights the possibility of determining the shear stress distribution along the skin of a pile, which represents skin resistance. Geotechnical engineering is plagued by the challenge of designing appropriate piles as a sufficient foundation construction while being economically justified solution. Static load testing facilitates verification if the pile satisfies these requirements. In most cases, the pile skin resistance is undervalued. This study first introduces the general approach based on static load test results using an appropriate mathematical approach in the presence of linear, vertical shear stress distribution boundary conditions as well as phenomena such as pile shortening and Kirchhoff's principle. Moreover, a scientific approach for pile compression and shear stress distribution is presented. Further, the study expands upon previous work by applying mathematical calculus to displacement piles. The promising results indicate that further work on greater number of piles may lead to a better understanding of pile–soil interaction and a more accurate design process.

Keywords: pile–soil interaction; skin resistance, pile-bearing capacity; load–settlement curve.

1 Introduction

Pile–soil interactions have been discussed since the 1940s [2; 30]. The bearing capacity of piles can be estimated using various methods [1; 3; 8; 26; 32]. The most widely known are based on static load test results [4; 5; 18] and transformational functions [12; 13; 19]. The author of the present study developed a method based on the Meyer–Kowalów (M–K) curve [20], which includes the static load test results and allows the vertical distribution of the skin shear stress as a boundary condition in numerical solutions. In this approach, the following mathematical descriptions are applied:

1. $$dN = \pi D \bullet \tau dz \tag{1}$$
2. Pile–soil interaction is described using Kirchhoff's principle [22] in accordance with the graph shown in Fig. 1.

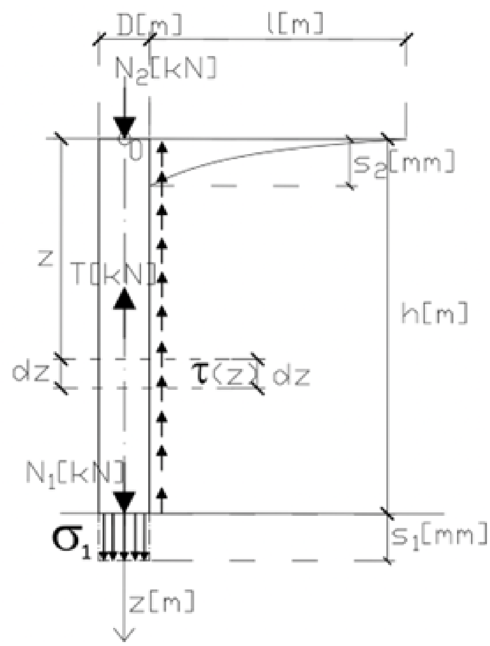

Figure 1: Graphical description of the loads acting on a pile in the presented approach. D – Pile diameter [m]; h – Pile length [m]; N_2 – Load acting on the head of the pile [N]; N_1 – Soil reaction at the toe [N]; T – Pile skin resistance [N]; $s_{2,1}$ – Settlement value of the head and base of the pile [mm]; σ_1 – Stress under the base of the pile [Pa]; τ – Stress acting on the skin of the pile, representing the skin resistance [Pa]; l – Arm of the soil deformation according to Kirchhoff's principle [m].

3. The relationship between the pile rigidity and the soil elasticity modulus $E_{s,v}/Ec$ is represented by a constant a. For the convenience of further calculation, it is introduced in the mathematical calculations. The pile dimensions, pile material, and soil properties can be used to estimate the relevant values:

***Corresponding author: Paweł Siemaszko,** Zachodniopomorski Uniwersytet Technologiczny w Szczecinie, Szczecin, Poland, E-mail: pw.siemaszko@gmail.com

$$a^2 = \frac{4G}{D \cdot E_c \cdot l} \quad (2)$$

$$G = \frac{E_{s,\upsilon}}{2(1+\upsilon)} \quad (3)$$

G – Shear modulus of the soil along the skin of the pile material [Pa]; E_c – Elastic modulus of the material [Pa]]; $E_{s,\upsilon}$ – Soil elasticity modulus along the pile skin [Pa]; υ – Poisson's coefficient of the soil along the skin of the pile [-]

4. These assumptions can help determine the linear distribution of the pile skin resistance, which is presented later herein.

In contrast to the approaches presented in literature, which discuss, for example, skin resistance calculations based on a centrifuge model [7], the method used in this study describes the mechanism of pile skin resistance mobilization as a result of the soil deformation under the load applied to the head of the pile and the axial force variation in the pile. Author intentionally decline to define the skin resistance as the result of the friction occurring between the pile and the soil. This friction is considered to occur after the boundary skin resistance value is surpassed when the soil starts to slide along the pile skin, which may decrease the actual pile-bearing capacity. It has been suggested that the residual stress should be included when calculating the pile-bearing capacity [6]. The omission of this effect is considered a mistake. This study did not directly use the force of the soil friction. Instead, it considered the mechanism of the bending of the soil space around the pile according to Kirchhoff's principle, which allowed to consider the entire soil body. An analysis of the experimental results showed that the applied mathematical description validates the presented approach [28]. The verification of the static load test results showed a positive correlation between the calculation and the field investigation results [22]. Multiple studies have been conducted on specific soil geotechnical parameters based on static load testing [9; 14; 15; 25; 33]. Piles technology affects the surface of pile skin, which should be considered in the design approach [29; 31].

Because the analysis is based on a set of piles, the research is extended to more field tests, including static load tests equipped with extensometers, to measure the pile-length shortening and verify the possibility of using the method in a wider range of cases. The piles that are considered have been the subjects of two notable studies [16; 17] and appear to be the most reliable for verification.

2 Description of Static Load Test Experiments and Results

The additional static load tests conducted were part of a project conducted in Northern Poland, Szczecin, Leona Heyki 3, near the Odra River. The approximate location is shown in Fig. 2.

Figure 2: Location of a static load test project in Northern Poland, Szczecin, Leona Heyki 3 street.

Static load tests were designed to determine the boundary-bearing capacity of the piles with an axial force distribution along the pile shaft. For this project, approximately 1,000 piles were ordered from a local developer [35]. Piles were designed with diameter D=0,4 [m] and length L=14,0-16,0 [m] depending on the placement in the area.

The test piles were equipped with extensometers to determine the axial distribution of the force $N(z)$ under a load N_2 applied to the pile head. Figure 3 shows the extensometer cables placed in the pile and the manner in which it is protected from damage.

Shown below are part of the results obtained during static load tests. Figure 5 presents the distribution of the axial force along the pile shaft and deformation measured during the static load test. In the scheme, there are placements of extensometers presented, along the reinforcement basket of the analyzed pile. Each of the analyzed pile had prefabricated reinforcement baskets with measurement devices attached, and they were placed in the pile after it was bored.

The author was present during the preparation period and static load process. I believe that performing natural-scale tests in field environments is the best way to verify

Figure 3: Pile designed for testing with visible extensometers attached to the reinforcing steel while casting (image captured by the author).

Figure 4: Part of the site prepared for static load testing (image captured by the author).

the theoretical assumptions. Figure 4 shows one of the static load test stations after the casting of necessary piles to perform a single test. All the piles used to perform the tests needed to achieve their design before constructing the stand are shown in Fig. 6.

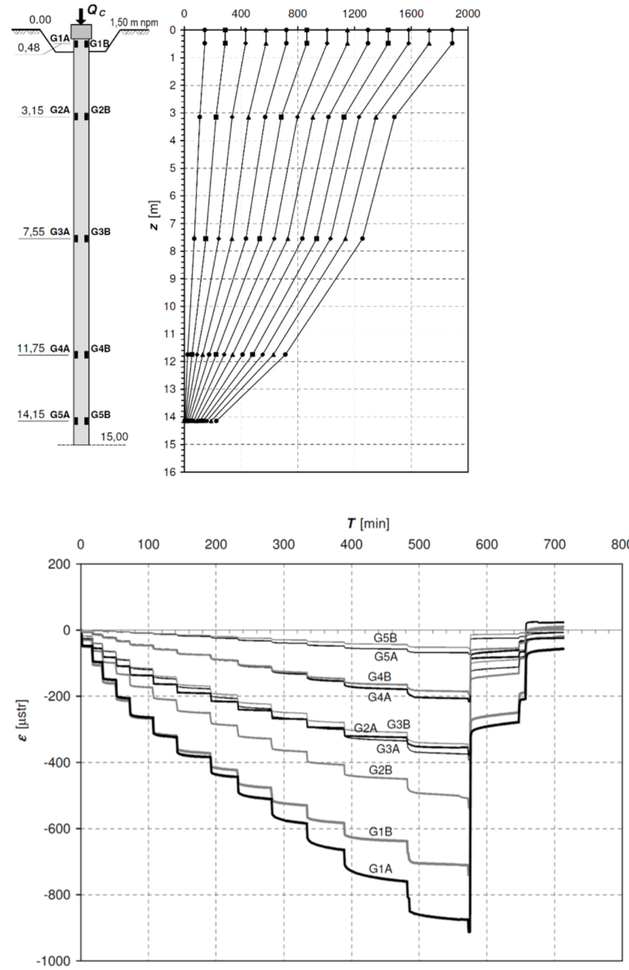

Figure 5: Distribution of the axial force along the pile shaft and deformation of the pile shaft measured during the static load test with extensometers [36].

Figure 6: Completed static load test site ready for testing (image obtained from authors' library).

Table 1: Load–settlement values obtained from the static load test; Pile Heyki 1.

N [kN]	0	145	289	432	576	720	863	1007	1150	1295	1438	1581	1726	1890
s [mm]	0,00	0,57	1,14	1,86	2,64	3,69	4,82	6,54	8,38	10,83	13,38	16,41	20,28	26,08

N: measured load applied to the pile head [kN]; *s*: measured settlement [mm]

Table 2: Load–settlement values obtained from static load test for Pile Heyki 2.

N [kN	0	145	293	431	575	720	864	1006	1151	1294	1438	1582	1726	1896	2013	2156	2300
s [mm]	0,00	0,71	1,27	1,88	2,57	3,49	4,48	6,04	7,77	10,24	13,24	16,13	19,59	23,20	27,14	31,73	36,42

N: measured load applied to the pile head [kN]; *s*: measured settlement [mm]

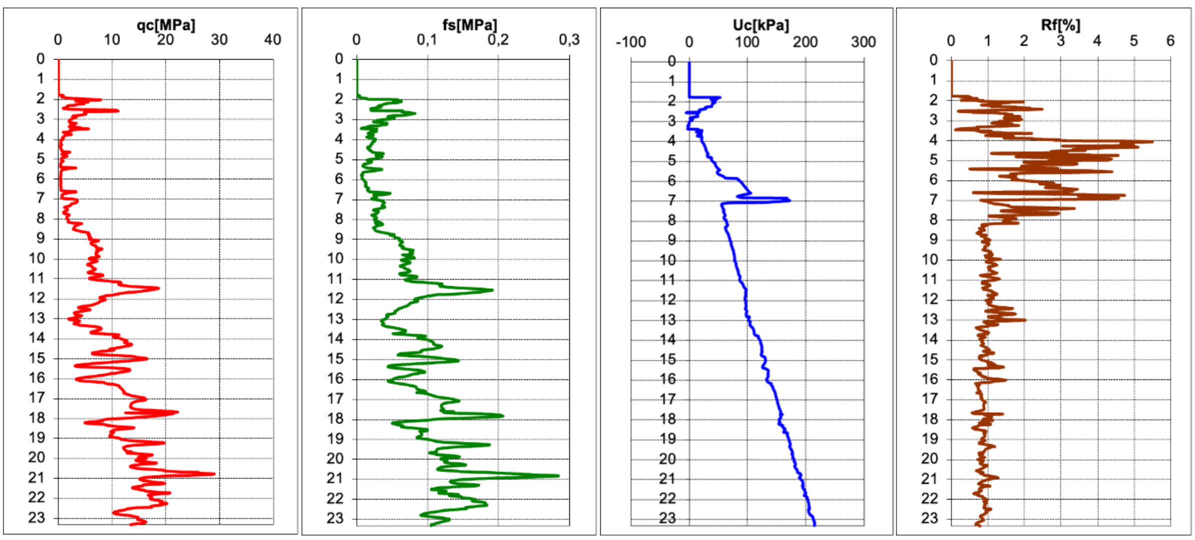

Figure 7: CPTu investigation results for Pile 1 [27].

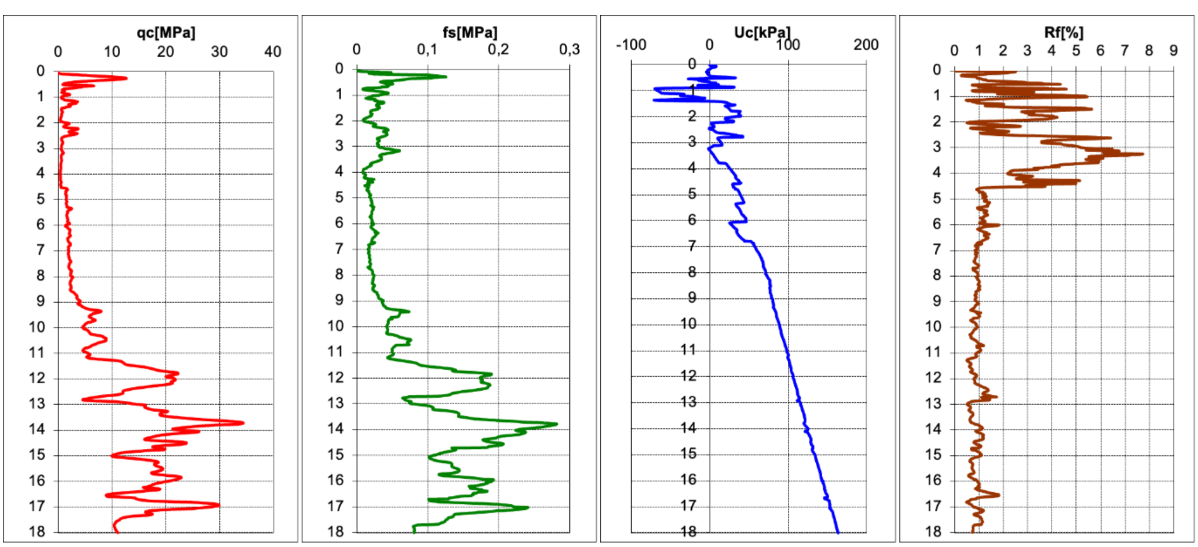

Figure 8: CPTu investigation results for Pile 2 [27].

Table 3. Geotechnical parameters of the soil profile [27].

			q_c	s_{vo}	I_D	I_c	q_n	β_q	N_m	Φ’	C’	Su(Cu)	M_0
[m]	[-]	[-]	[MPa]	[KPa]	[%]	[-]	[MPa]	[-]	[-]	[°]	[kPa]	[kPa]	[MPa]
0,0													
1,8	Mg(hgrcFSa)	nN(Pd+H+c+ż)	2,20	35	20	-	2,19	0,02	-	29° 30’	-	-	9,5
2,3	Mg(grchclSa)	nN(Pg+H+c+ż)	1,30	42	-	0,54	1,27	0,01	11,1	22° 10’	6	98	9,2
2,5	Mg(grchFSa)	nN(Pd+H+c+ż)	2,20	57	15	-	2,14	0,00	-	29°	-	-	9,4
3,8	Or(Nm)	Nm	0,45	92	-	0,50	0,38	0,04	3,7	13° 10’	3	20	1,1
6,6	Or(Nm)	Nm	0,65	117	-	0,60	0,58	0,12	5,1	15° 50’	4	31	2,5
7,0	Or(Nmp)/HFSa	Nmp/PdH	1,10	133	-	0,44	1,00	0,01	6,8	18° 50’	5	71	7,9
8,2	FSa	Pd	3,30	149	20	-	3,18	0,00	-	29° 20’	-	-	14,2
8,6	FSa	Pd/Ps	6,40	177	40	-	6,25	0,00	-	32° 10’	-	-	28,4
11,1	FSa	Pd	13,20	208	65	-	13,03	0,00	-	35° 10’	-	-	64,9
11,8	FSa	Pd	7,30	220	40	-	7,12	0,00	-	32° 20’	-	-	32,4
12,4	saSi	Πp	2,60	236	-	0,74	2,40	0,00	11,1	22° 10’	7	171	21,8
13,3	FSa	Pd	7,00	250	35	-	6,80	0,00	-	31° 50’	-	-	31,1
13,8	FSa	Pd	11,10	268	55	-	10,88	0,00	-	33° 50’	-	-	54,6
15,2	saSi/siSa	Πp/Pπ	3,40	292	-	0,82	3,17	0,00	12,2	22° 50’	7	226	28,5
16,2	FSa/MSa	Pd/Ps	14,00	320	60	-	13,74	0,00	-	34° 30’	-	-	70,3
18,0	FSa	Pd	7,00	342	30	-	6,73	0,00	-	31°	-	-	31,2
18,4	FSa	Pd	10,50	353	45	-	10,22	0,00	-	33°	-	-	51,8
19,1	FSa/MSa	Pd/Ps	15,40	400	60	-	15,08	0,00	-	34° 30’	-	-	75,9

Displacement piles were used to determine whether previous calculations could be applied to other piling technologies, as previous work focused on CFA piles [22]. Tables 1 and 2 present the static load test results. Figures 7 and 8 present the results of the CPTu investigation. Table 3 presents the geotechnical parameters of the soil profile.

3 Mathematical Description of the Problem

3.1 Meyer–Kowalów Curve Concept

The Meyer–Kowalów curve concept has been introduced and widely applied [20; 23; 24]. It is based on soil mechanics principles [10]. This method allows the extrapolation of a static load test curve to estimate the boundary-bearing capacity of the pile (N_{gr}). The curve can be described using C, N_{gr2}, and k. Parameter C is introduced as an aggregation of the toe and skin resistances during pile settlement. The following equation is used to extrapolate the static load test curve in the M–K method:

$$s = C \cdot N_{gr} \cdot \frac{\left(1 - \frac{N}{N_{gr}}\right)^{-\nu} - 1}{\nu} \tag{4}$$

s – Settlement of the head of the pile [mm]; C – Reversed aggregated Winkler modulus $[m/MN]$ [21]; N_{gr} – Axial force, M–K curve vertical asymptote [MN]; k – Parameter showing the proportions of base and shaft resistances [-]

The M–K curve exhibits a vertical asymptote:

$$N = N_{gr} \text{ and diagonal} \tag{5}$$

$$s = C \cdot N \tag{6}$$

It can be proven that:

$$\lim_{N \to 0} s(N) = C \cdot N \text{ and} \tag{7}$$

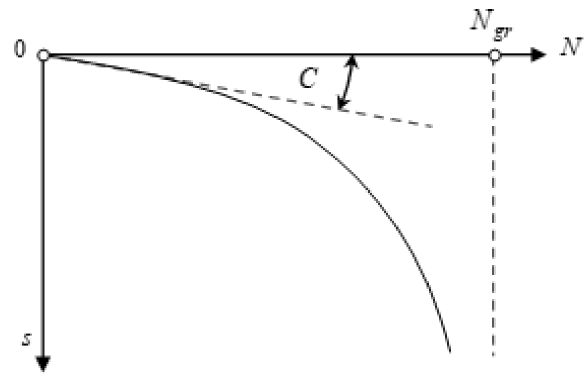

Figure 9: Example of the M–K curve graph [20].

$$\lim_{N \to N_{gr}} s(N) = \infty \tag{8}$$

Figure 9 shows an example of the M–K curve graph.

The M–K curve depicts the physical aspects of pile settlement as an effect of the axial load acting on the pile head. For $N \longrightarrow 0$, a small displacement and linear characteristic of the load–settlement relationship could be observed. For $N \longrightarrow N_{gr}$, the settlement increased uncontrollably, and the pile lost its bearing capacity. The M–K curve parameters were estimated statistically using a set of load–settlement values $\{s_i; N_i\}$.

The principle behind the M–K curve approximation is the estimation of the N_{gr} value and the prediction of the mobilization of the pile base and shaft capacity. The curve presented by Chin [5] is a variation of the M–K curve, where $\kappa = 1$.

The M–K curve facilitated the estimation of the extreme value of the skin resistance of the pile. Briaud and Tucker [2] concluded that estimating the boundary resistance of a pile yields better results than predicting the settlement.

3.2 Pile toe and skin resistance formation

It is assumed that the skin resistance can be expressed using the shear stress $\tau(z)$, which is the result of the axial force acting on the head of the pile and its variation along the shaft.

$$dN = \pi D \bullet \tau dz \tag{9}$$

This is the result of the equilibrium of the axial forces in the pile. The shear stress $\tau(z)$ in the soil around the pile is the result of bending the soil body in the range of "l" from the pile head caused by its settlement. Kirchhoff's principle can be expressed as follows:

$$G = \frac{E_{s,v}}{2(1+\upsilon)} \tag{10}$$

G – Kirchhoff's modulus of the soil along the skin of pile [Pa]; E_c – Elasticity modulus of the concrete piles [Pa]; $E_{s,v}$ – Soil elasticity modulus along the pile skin [Pa]; υ – Poisson's coefficient for soil along the skin of the pile [-].

Furthermore:

$$s(z) = \frac{\tau(z) \cdot l}{G} \tag{11}$$

Another phenomenon that must be considered in the calculations is the pile-shortening effect caused by the axial force $N(z)$ from a depth z=0 to z=h, assuming an elastic deformation of the pile:

$$s_*(z) = \frac{4}{\pi D^2 E_c} \cdot \int_0^z N(z) dz \tag{12}$$

It is assumed that pile–soil interaction can occur without soil slipping along the pile skin, which has been verified in previous research [21]:

$$s(z) - s_*(z) = 0 \tag{13}$$

Pile skin shear stress $\tau(z)$ is unrelated to the phenomenon of soil slipping along the pile shaft and the soil stress component perpendicular to the shaft. This depends on Kirchhoff's principle of the bending space around the pile.

Surpassing the maximal static friction between the skin of the pile and the soil results in a terminal skin resistance and soil-slipping effect. The proposed mathematical model is based on the following assumptions:

– Skin resistance is presented as the shear stress $\tau(z)$.
– Shear stress along the pile's skin is described using Kirchhoff's principle.
– Pile shortening is described as an elastic deformation process.
– There is no slipping effect of the soil along the pile's skin.

With these assumptions, a differential equation for the axial change in the shear stress against the vertical coordinate "z" can be obtained:

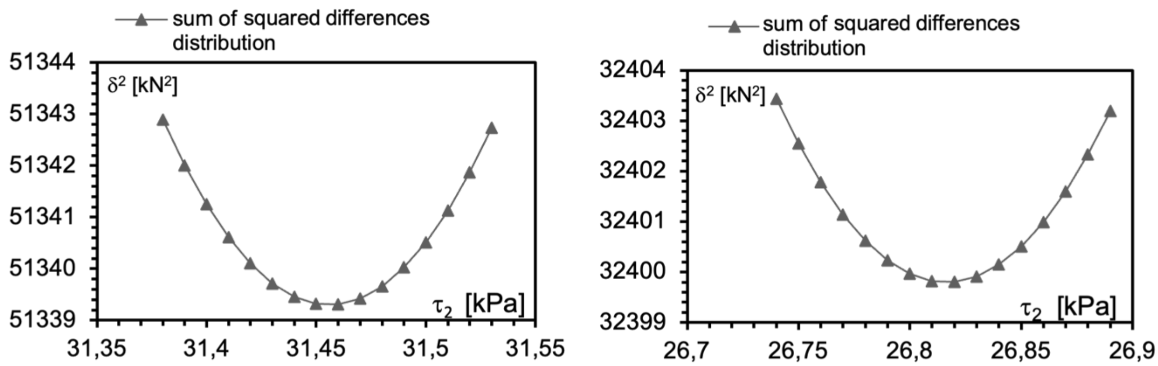

Figure 10: Least-squares graphs of the results obtained for the analyzed piles.

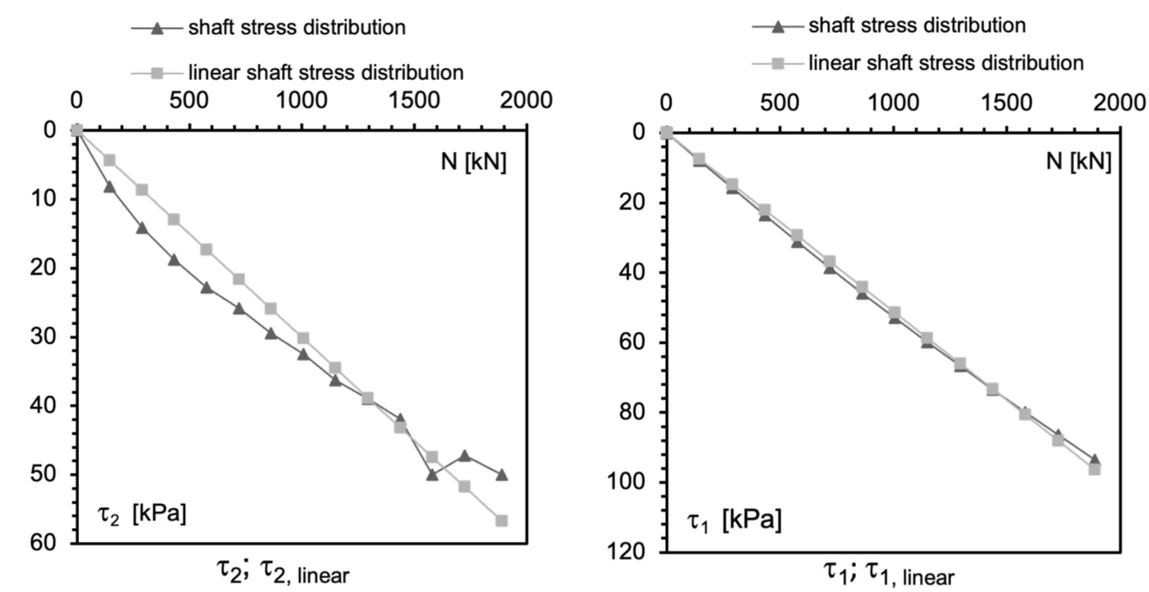

Figure 11: Relationship between the load acting on the head of the pile and the shear stress at the head level (τ_2) and base level (τ_1) for the pile taken from Heyki 1 [by author].

$$\frac{d^2\tau}{dz^2} = \frac{4G}{l \cdot D \cdot E_c} \cdot \tau \tag{14}$$

The a coefficient, defined in Eq. (2), yields:

$$\frac{d^2\tau}{d(a \cdot z)^2} - \tau = 0 \tag{15}$$

The solution to this equation can be expressed as follows:

$$\tau(z) = A_1 \sinh(az) + A_2 \cosh(az) \tag{16}$$

The boundary conditions of the solution are z=0; τ=τ_2 and z=h; τ=τ_1. A detailed analysis of the solution presented in previous research [22] showed that the influence of the a coefficient, expressed in (2), does not have a carryover effect on the shear stress distribution. This verification confirms the possibility of applying such a simplification. The author estimated the value of constant a in a practical environment, producing results close to 0.05 [1/m]. Considering these results, the linear distribution of $\tau(z)$ along the skin of the pile can be obtained as follows:

$$\tau(z) = \tau_2 - (\tau_2 - \tau_1)\sqrt{\left(\frac{z}{h}\right)} \tag{17}$$

The axial change in $N(z)$ can be expressed as follows:

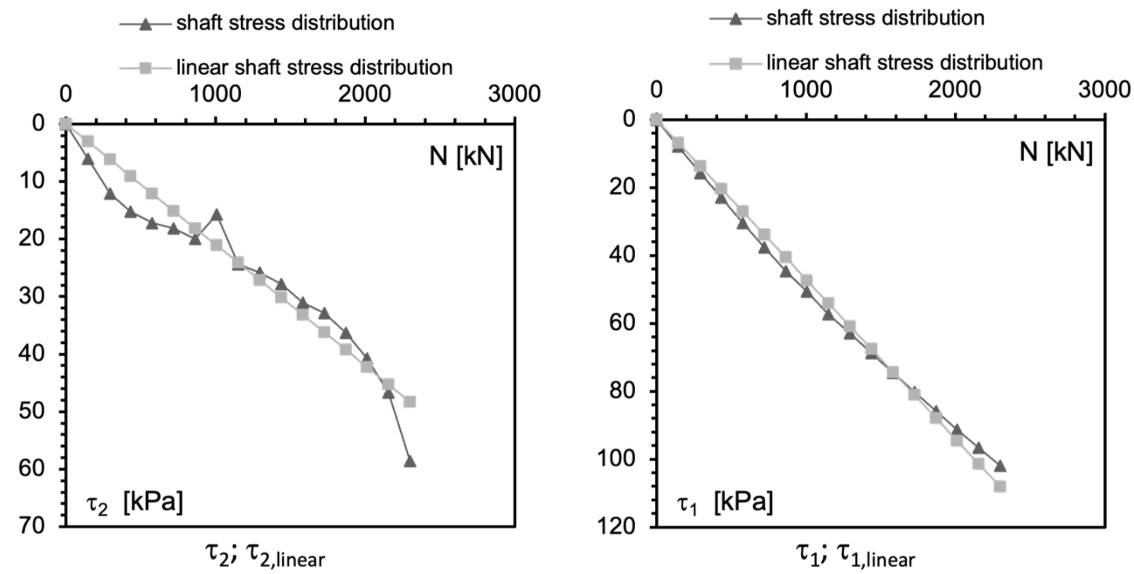

Figure 12: Relationship between the load acting on the head of the pile and the shear stress at the head level (τ_2) and base level (τ_1) for the pile taken from Heyki 2 [by author].

$$N(z) = N_2 - \pi D h \cdot \left[\tau_2 \cdot \left(\frac{z}{h}\right) - \frac{1}{2}(\tau_2 - \tau_1) \cdot \left(\frac{z}{h}\right)^2\right] \quad (18)$$

This equation was used to verify the $\tau(z)$ axial distribution in the analyzed case and was applied to the experimental analysis of the field experiments. In previous studies [22; 28], it was important to determine if there is a possibility of omitting the influence of the *a* value and assuming *a*=*const*. The verification results showed that including the value constant *a* produced a good correlation with the graphs, where its influence was omitted. Meyer and Siemaszko [22] and Siemaszko [28] reported this correlation.

4 Analysis of the Field Static Load Test Results

Siemaszko [28] performed an essential analysis of the results obtained from static load testing based on (18). Least-squares graphs were obtained to verify whether the static load test results can be presented as a linear distribution. The general form of the least-squares method is as follows:

$$\delta^2 = \sum \left(x_{i,m} - x_{i,c}\right)^2 = min \quad (19)$$

δ^2– Squared sum of the differences between the measured and calculated results—values of the load $N(z)$ from the static load test and calculated using Eq. (18).
$x_{i,m}$ – Measured values [mm]
$x_{i,c}$ – Calculated value [mm]

In this study, the results of the least-squares method analysis showed extreme values and normal distributions, as shown in Fig. 10.

This analysis allowed to draw graphs of the shear stress distribution using the mathematical approach presented by Siemaszko [28]. Figures 11 and 12 show the graphs obtained for the piles analyzed in this study.

4.1 Values of $\tau_1(N_2)$ and $\tau_2(N_2)$ estimated by practical calculations

The author proposed an equation for the practical calculations of τ_1 and τ_2. Following the shear stress τ_1 calculations conducted in a previous experimental analysis by [11], the following equation is included:

$$\tau_1 = \frac{4 \cdot N_2}{\pi D^2} \cdot f \frac{\tan^2\left(45 - \frac{\phi}{2}\right)}{\tan^2\left(45 + \frac{\phi}{2}\right)} \quad (20)$$

In this equation, f is the kinematic friction coefficient, and ϕ is the internal friction angle of the soil in its natural state.

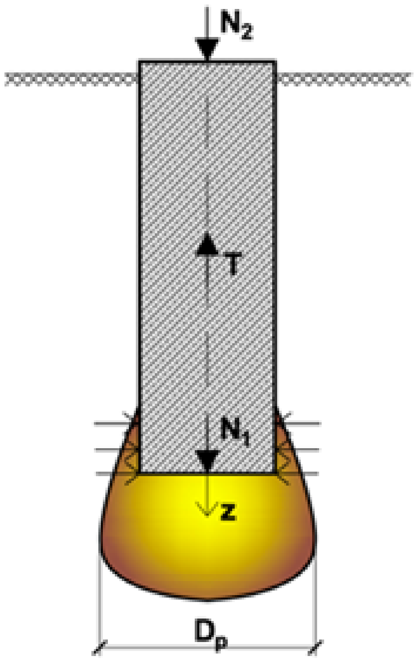

Figure 13: Soil under and around the pile base forming a sphere, where the parameters vary significantly [22, 28].

This analysis showed that influencing the force applied to the soil by the pile base results in changes within its structure, and therefore, its geotechnical properties. The changed properties can be represented as $f \longrightarrow f_*$ and $\phi \longrightarrow \phi_*$.

$$\tan^2\left(45+\frac{\phi_*}{2}\right)=\sqrt{1+\kappa_2} \tag{21}$$

This yields the following:

$$\phi_* = 2\cdot\left[\arctan\left(\sqrt{1+\kappa_2}\right)-45^o\right] \tag{22}$$

For the practical purpose of performing engineering calculations with sufficient accuracy, Equation (22) can be expressed as follows:

$$\phi_* = 18{,}31\cdot\kappa_2^{0{,}715} \tag{23}$$

where ϕ_* is in degrees.

For the soil under the pile base, both the internal shear angle and the dynamic friction coefficient vary. With these changes applied, the following equation for the shear stress τ_1 can be used:

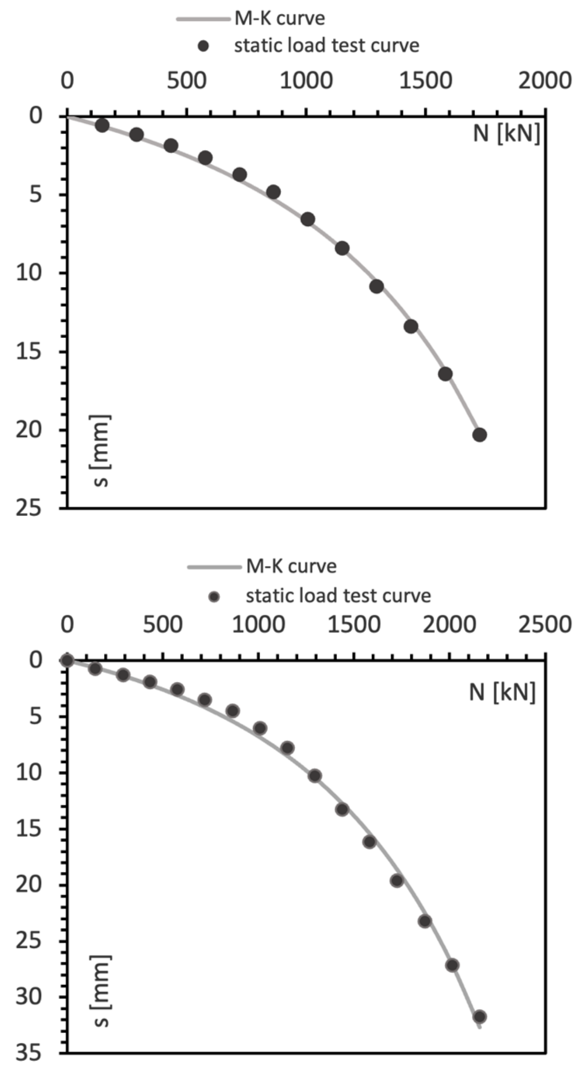

Figure 14: M–K curve and static load test results compared for Pile 1 (left) and Pile 2 (right).

$$\tau_1 = \frac{4\cdot N_2}{\pi D^2}\cdot f_*\frac{\tan^2\left(45-\frac{\phi_*}{2}\right)}{\tan^2\left(45+\frac{\phi_*}{2}\right)} \tag{24}$$

The equation that includes both $f \longrightarrow f_*$ and $\phi \longrightarrow \phi_*$ can be presented as follows:

$$\tau_1 = \frac{4\cdot N_2}{\pi D^2}\cdot\frac{f\cdot\kappa_2}{(1+\kappa_2)^4} \tag{25}$$

Equation (25) is the primary relationship, including the phenomena at the base of the pile with varying soil properties, as shown in Fig. 13.

Another calculated value is τ_2, which is the shear stress at the head of the pile. The following boundary

Table 4: Equation (42) results, left side and right side.

	Left side EQ. (42)	Right side Eq.(42)
Pile 1	0,83	0,803
Pile 2	0,85	0,84

conditions were assumed: for z=0, there is $\tau(z)=\tau_2$; for $z=h$, there is $\tau(z)=\tau_1$. The vertical force equilibrium is expressed as follows:

$$T = N_2 - N_1 \tag{26}$$

From the linear distributions of the shear stress and pile skin resistance, the following can be assumed:

$$T = \frac{\pi DH(\tau_2 + \tau_1)}{2} \tag{27}$$

Using the M–K curve theory, the following relationships can be obtained for rough calculations:

$$N_1 = \frac{N_2}{(1+\kappa_2)^2} \tag{28}$$

$$\tau_2 + \tau_1 = \frac{2N_2}{\pi DH} \cdot \frac{\kappa_2}{(1+\kappa_2)^2} \cdot \left[2 + \kappa_2 - \frac{2Hf}{D} \cdot \frac{1}{(1+\kappa_2)^2}\right] \tag{29}$$

For further analysis, the α coefficient is substituted into the equation:

$$\alpha = \frac{2Hf}{D} \tag{30}$$

The final equations for τ_2 and τ_1 are as follows:

$$\tau_1 = \frac{4N_2}{\pi D^2} \cdot \frac{f \cdot \kappa_2}{(1+\kappa_2)^4} \tag{31}$$

$$\tau_2 = \frac{2N_2}{\pi DH} \cdot \frac{\kappa_2}{(1+\kappa_2)^2} \cdot \left[2 + \kappa_2 - \frac{\alpha}{(1+\kappa_2)^2}\right] \tag{32}$$

Thus, the relationships presented above were verified. Figures 11 and 12 show the values of $\tau(z)=\tau_2$ and $\tau(z)=\tau_1$. As the distributions presented in the graphs suggest a linear correlation between $\tau_2(N_2)$ and $\tau_1(N_2)$, the following relationships can be applied:

$$\tau_1 = A_1 \cdot N_2 \tag{33}$$

$$\tau_2 = A_2 \cdot N_2 \tag{34}$$

The coefficients A_1 and A_2 were estimated using the least-squares method for both the piles. For both the piles, statistical calculations were performed to obtain the M–K curve parameters N_2, C_2, and κ_2. The results of the *Q-s* curves obtained using the M–K curve method are shown through the graphs in Fig. 14.

A comparison was made between the values A_1 and A_2 calculated from the experimental results obtained under natural conditions and the values obtained using the M–K curve method.

$$\tau_1 = \frac{2N_2}{\pi DH} \cdot \frac{2Hf \cdot \kappa_2}{D(1+\kappa_2)^4} = \frac{2N_2}{\pi DH} \cdot \frac{2Hf \cdot \kappa_2}{D(1+\kappa_2)^4} \tag{35}$$

$$\alpha = \frac{2Hf}{D} \tag{30}$$

$$\tau_2 = \frac{2N_2}{\pi DH} \cdot \frac{\kappa_2}{(1+\kappa_2)^2} \cdot \left[2 + \kappa_2 - \frac{\alpha}{(1+\kappa_2)^2}\right] \tag{36}$$

The experimental results can be described as follows:

$$A_1 = \frac{2 \cdot \kappa_2}{\pi DH} \cdot \frac{\alpha}{(1+\kappa_2)^4} \tag{37}$$

$$A_2 = \frac{2 \cdot \kappa_2}{\pi DH} \cdot \frac{1}{(1+\kappa_2)^2}\left[2 + \kappa_2 - \frac{\alpha}{(1+\kappa_2)^4}\right] = A_1 \cdot \frac{(1+\kappa_2)^2\left[2 + \kappa_2 - \frac{\alpha}{(1+\kappa_2)^2}\right]}{\alpha} \tag{38}$$

4.2 Verification of the linear relationships $\tau_1(N_2)$ and $\tau_2(N_2)$

The author attempted to verify the linear dependency between the head load N_2 and the skin shear stresses τ_1 and τ_2. The following solutions were used based on the experimental field test results:

$$\tau_1 = \tau_1(N_2) = A_1 \cdot N_2 \tag{39}$$

$$\tau_2 = \tau_2(N_2) = A_2 \cdot N_2 \tag{40}$$

Here, A_1; A_1=*const*. As for the equilibrium of the axial forces, it is:

$$N_2 - N_1 = \frac{\tau_1 + \tau_2}{2} \cdot \pi DH \tag{41}$$

The equations include the linear characteristic of the shear stress acting on the skin of the pile $\tau(z)$, which represents the skin resistance [22]. Based on the analysis previously conducted based on the M–K theory, Eq. (28) is valid. This can be used to obtain the following relationship:

$$N_2 \cdot \left[1 - \frac{1}{(1+\kappa_2)^2}\right] = \frac{A_1 \cdot N_2 + A_2 \cdot N_2}{2} \cdot \pi DH \tag{42}$$

Therefore:

$$1 - \frac{1}{(1+\kappa_2)^2} = \frac{A_1 + A_2}{2} \cdot \pi DH \tag{43}$$

The values obtained for Piles 1 and 2 are presented in Table 4.

Using the above equation, the κ_2 parameter value for the results can be verified, including the value of the pile-shortening effect. However, the value of the κ_2 parameter may not be equal to κ_2 derived from $\{s_i;N_i\}$ obtained using statistical calculations. This suggests that the principles of earlier research [34] require further verification.

5 Conclusions

This study presents an analytical approach verified by conducting field experiments at a natural scale. Studies have focused on describing the mechanisms of the formation of skin resistance. Piles were designed and executed as soil-displacement piles. The study results confirmed that the pile-shortening effect may be applied to calculations, resulting in a linear shear stress distribution, which represents the pile skin resistance. The experimental research and analytical evaluation showed that τ_1 and τ_2 exhibited a linear dependency with the load acting at the head of the pile N_2. This further led to the conclusion that the skin resistance, which is based on τ_1 and τ_2, is also linearly dependent on N_2. Presented study results may be useful in solving geotechnical problems using numerical solution packages. Linear differential equations have been solved using the method proposed by Leibnitz in 1852. However, to solve these differential equations, the distribution of the function along the boundary of the figure of solution must be known. The linear distribution, which is the result of the research presented in this study, can be used as a boundary condition to solve the strain distribution problem using numerical methods. The analysis showed a positive correlation between the M–K method parameters, calculated statistically based on $\{s_i;N_i\}$ values, and the approach based on the pile-shortening effect, which allows the determination of the shear stress along the pile skin. The research focused on verifying the applicability of a linear distribution of the shear stress to soil displacement piles, similar to that applied to CFA piles, which has been verified in previous research. The results of this study can be improved by analyzing a greater number of piles. The performance of static load tests until failure using additional measurement devices is financially demanding and limits the acquiring of sufficient amount of these results. Currently, there is ongoing preparation of a suitable construction methodology that will facilitate the conduction of static load tests close to the natural scale environments within a shorter time frame. Initial attempts have yielded promising results. Future work will be focused on the analysis of a greater number of piles to achieve a better understanding of the pile–soil interaction and further improve the developed calculus.

References

[1] Azzouz, A. S., M. M. Baligh, and A. J. Whittle. 1990. “Shaft resistance of piles in clay.” *J. Geotech. Eng.* 116(2): 205–221.

[2] Briaud, J. and L. Tucker. 1984. “Piles in sand: A method including residual stress.” *J. Geotech. Eng.* 110(11): 1666–1680.

[3] Briaud, J. L. 2013. “Geotechnical engineering: Unsaturated and saturated soils.” Wiley, New Jersey.

[4] Brinch Hansen, J. 1970. “A revised and extended formula for bearing capacity.” Danish Geotechnical Institute, Bull, Copenhagen.

[5] Chin, F. K. 1970. “Estimation of ultimate load of piles not carried to failure.” Proceedings 2nd Southeast Asia Conference on Soil Engineering: 81–92.

[6] Di Donna, A., A. Ferrari, and L. Laloui. 2016. “Experimental investigations of the soil–concrete interface: Physical mechanisms, cyclic mobilization, and behaviour at different temperatures.” *Can. Geotech. J.* 53: 1–14. *http://dx.doi.org/10.1139/cgj-2015-0294*

[7] Fioravante, V. 2002. "On the shaft friction modelling of non-displacement piles in sand." *Soils Found.* 42(2): 23–33.

[8] Fleming, W. G. K. 1992. "A new method for single pile settlement prediction and analysis." *Géotechnique* 42(3): 411–425.

[9] Galvis-Castro, A. C., D. Tovar-Valencia Ruben, R. Salgado, and M. Prezzi. 2019. "Compressive and tensile shaft resistance of nondisplacement piles in sand." *J. Geotech. Geoenviron. Eng.* 145(9): 04019041.

[10] Glazer, Z. 1977. "Mechanika gruntów" *in Polish*. Wydawnictwa Geologiczne, Warszawa.

[11] Gumny, K., PhD. 2021. "Soil-structure interaction in single pile-raft foundation." West Pomeranian University of Technology in Szczecin, Szczecin.

[12] Gwizdała, K. 1996. "Analiza osiadań pali przy wykorzystaniu funkcji transformacyjnych" *in Polish*. Zeszyty Naukowe Politechniki Gdańskiej, Nr 532, Budownictwo Wodne Nr 41.

[13] Gwizdała, K., and M. Stęczniewski. 2015. "Wykorzystanie metody funkcji transformacyjnych do analizy nośności i osiadań pali CFA" *in Polish*. *Inżynieria Morska i Geotechnika* 2015(3): 433–437.

[14] Ismael, N. F. 1989. "Skin friction of driven piles in calcareous sands." *J. Geotech. Eng.* 115(1): 135–139.

[15] Jardine, R. J., R. Standing Jr., and F. Chow. C. 2006. "Some observations of the effects of time on the capacity of piles driven in sand." *Géotechnique* 56(4): 227–244.

[16] Lee, C. Y., and H. G. Poulos. 1991. "Tests on model instrumented grouted piles in offshore calcareous soil." *J. Geotech. Eng.* 117(11): 1738–1753.

[17] Lehane, B. M., R. J. Jardine, A. J. Bond, and R. Frank. 1993. "Mechanisms of shaft friction in sand from instrumented pile tests," *J. Geotech. Eng.* 119(1): 19–35

[18] Le Kouby, A., J. C. Dupla, J. Canou, and R. Francis. 2013. "Pile response in sand: Experimental development and study." *Int. J. Physical Model. Geotech.* 13(4): 122–137.

[19] Mazurkiewicz, B. 1966; "Sprawdzanie dopuszczalnej nośności pali w terenie. Cz. 2" *in Polish*. *Inżynieria i budownictwo n*r 6: 214–218.

[20] Meyer, Z., and M. Kowalów. 2010. "Model krzywej aproksymującej wyniki testów statycznych pali" *in Polish*. *Inżynieria Morska i Geotechnika* 3: 438–441.

[21] Meyer, Z., and P. Siemaszko. 2019. "Static load test analysis based on soil field investigations." *Bull. Pol. Acad. Sci.: Tech Sci.* 67(2): 329–337.

[22] Meyer, Z., and P. Siemaszko. 2021. "Analysis of the pile skin resistance formation." *Studia Geotechnica et Mechanica* 43(4): 380–388.

[23] Meyer, Z., and K. Stachecki. 2018. "Static load test curve (Q–s) conversion in to pile of different size." *Ann. Warsaw Univ. Life Sci. – SGGW* 50: 171–182.

[24] Meyer, Z., and K. Żarkiewicz. 2018. "Skin and toe resistance mobilisation of pile during laboratory static load test." *Studia Geotechnica et Mechanica* 40: 1–5.

[25] Miller, G. A., and A. J. Lutenegger. 1997. "Influence of pile plugging on skin friction in overconsolidated clay." *J. Geotech. Geoenviron. Eng.* 123(6): 525–533.

[26] Mochtar, I. B., and T. B. Edil. 1988. "Shaft resistance of model pile in clay." J. Geotech. Eng. 114(11): 1227–1244.

[27] N-Geo. 2018. "Soil geotechnical parameters based on CPTu investigation." Part of the "Nowa Przystań" project documentation.

[28] Siemaszko, P., PhD. 2022. "Analysis of the pile shortening effect on skin resistance formation." West Pomeranian Institute of Technology in Szczecin, Szczecin.

[29] Tehrani, F. S., F. Han, R. Salgado, M. Prezzi, R. D. Tovar, and A. G. Gastro. 2016. "Effect of surface roughness on the shaft resistance of non-displacement piles embedded in sand." *Géotechnique* 66(5): 386–400.

[30] Terzaghi, K., and R. B. Peck. 1967. "Soil mechanics in engineering practice." Wiley and Sons, New York.

[31] Thilakasiri, H. S. 2007. "Qualitative interpretation of load-settlement curves of bored piles." *Eng.: J. Inst. Eng. (Sri Lanka)* 40(4): 61–68.

[32] Tomlinson, M., and J. Woodward. 2008. "Pile design and construction practice." Taylor and Francis London, New York.

[33] Zhang, C., G. D. Nguyen, and I. Einav. 2013. "The end-bearing capacity of piles penetrating into crushable soils." *Géotechnique* 63(5): 341–354. *http://dx.doi.org/10.1680/geot.11.P.117*

[34] Żarkiewicz, K., PhD. 2017. "Analysis of pile shaft bearing capacity formation in non-cohesive soils based on laboratory model investigation" *in Polish*. West Pomeranian University of Technology in Szczecin, Szczecin

[35] Project documentation by FBA for "Nowa Przystań" address Leona Heyki 3 Szczecin.

[36] Scientific description of the static load test results with extensometers for "Nowa Przystań" address Leona Heyki 3 Szczecin.